https://doi.org/10.2352/EI.2023.35.15.COLOR-208

Dot Profile Model-Based Direct Binary Search

***Yafei Mao** [a]**, Utpal Sarkar** [b]**, Isabel Borrell** [b]**, Lluis Abello** [b]**, Jan P. Allebach** [a]*
[a] ***School of Electrical and Computer Engineering, Purdue University, West Lafayette, IN 47907, U.S.A.***
[b] ***HP Inc., Sant Cugat del Valles, SPAIN***

Abstract

A dot profile model to compensate dot shape irregularity errors of inkjet printers is proposed. Previous tabular approaches for parameterizing the printer model rely on the measurements of the gray level of various printed halftone patterns. However, lots of patterns need to be printed and scanned if the printer generates large drops of colorant. To solve this problem, we propose to simulate the appearance of the rendered patterns so that the model parameters can be computed analytically. The simulation uses the mean dot as the printer dot profile and saturated addition to resolve dot overlap. Besides, we incorporate a standard definition (SD) and a high definition (HD) equivalent gray-scale representation of the printed halftone image produced by the dot profile model into the direct binary search (DBS) algorithm. Experimental results show great improvement in the mid-tone and shadow regions over the printed image halftoned by the original DBS. The HD model further enhances details in the shadows.

Introduction

Digital halftoning, an essential technique for printers, is the process of rendering a continuous-tone image with a limited number of tone levels. The direct binary search (DBS) algorithm as an iterative method, yields the best halftone reproductions [1]; so we are particularly interested in it.

Elementary halftoning algorithms assume that the ideal shape for the printed dots would be an $X \times X$ square, where X is the dot spacing in inches; so $1/X$ is the printer resolution in dpi (dots per inch). However, real-world printers typically produce dots that are larger and more irregular than that. If the algorithm does not account for such printer distortions, the resulting print may contain annoying textures and distorted gray levels.

Several studies have focused on model-based techniques to mitigate printer effects. The main idea is to establish a model to predict the actual gray value of each pixel in the printed image. A popular model is the hard circular dot (HCD) model proposed in [2]. In this model, each printed pixel is assumed to be a circular spot with constant absorptance, and multiple dot overlap is resolved as a logical OR [3–6]. The HCD model can be used in DBS to enhance tonal reproduction and detail rendition [7, 8]. Pappas et al [9] proposed a tabular model based on the macroscopic measurements of a set of printed binary patterns in a neighborhood. Baqai et al [8] simplified the approach by using the microscopic measurement of the center pixel of all possible patterns in the neighborhood. A similar idea based on the tabular model was presented in [10]. More recently, Zhang et al focused on predicting the printed text strokes and compensated thickened edges after halftoning and before printing [11]. Liu et al parameterized a laser printer model for the error diffusion algorithm [12]. Work in [13] utilized a physics model to estimated the ink reflectance.

Though these models have achieved successful results, there still are some limitations in their applicability. Some models were developed for a different halftoning algorithm, so they cannot be applied to DBS. As for the DBS printer models, the HCD model might be incompatible with printers that do not produce perfectly round and uniformly dark dots [14]. And the tabular models require extensive measurements for devices that render large dots of colorant. This is because the number of possible dot configurations grows exponentially as the neighborhood size increases.

Most of the aforementioned researches were oriented to laser electrophotographic (EP) printers where the dots are very sensitive to the EP process, such that the printer cannot reliably print isolated pixels [8, 15]. Accordingly, estimating the pixel absorptance has to rely on the interaction between adjacent pixels. In contrast, inkjet printers generally produce dots that are reasonably consistent and much more stable relative to those produced by EP printers [10]. Nevertheless, the ink dots may be irregularly shaped [16, 17], much larger than the minimal size [18], and misaligned [10]. This suggests the use of an analytical model rather than a completely measurement-based model for inkjet printers.

To address these issues, we propose an analytical dot profile model in which arbitrarily shaped non-flat dots are studied. To parametrize the model, we first compute the dot statistics, such as the mean and standard deviation profiles, based on the data collected from individual dots. By using saturated addition to describe the effect of dot overlap, the model parameters can be computed analytically as a function of the mean dot profile and the values of the adjacent pixels. This simplifies the printer characterization process considerably because we only need to measure a limited number of isolated dots. We also assume that the ink dots are centered on their nominal locations with no misplacement.

Our goal is to incorporate the dot profile model in DBS to suppress the print artifacts caused by dot shape irregularity errors. Additionally, motivated by [19], we present both a standard definition (SD) and a high definition (HD) model. These models enable DBS to examine the visual fidelity of the rendered halftone at the printer resolution and a 3-times higher resolution, respectively. Experimental results demonstrate that by using these dot profile models, DBS can effectively improve the quality of the printed image. In particular, the HD model further refines the appearance of the shadow regions.

Preliminaries
Notation

An SD printer pixel $[m,n]$ is an $X \times X$ square centered at the point (x_m, y_n) with $\{(x_m, y_n) : x_m = mX + \frac{X}{2}, y_n = nX + \frac{X}{2}\}$.

Research partially supported by HP Inc., Barcelona, SPAIN.

An HD pixel $[u,v]$ is a $\frac{X}{3} \times \frac{X}{3}$ square centered at (x_u, y_v) with $\{(x_u, y_v) : x_u = u\frac{X}{3} + \frac{X}{6}, y_v = v\frac{X}{3} + \frac{X}{6}\}$.

Printer Characterization

The first step towards printer modeling is to characterize the printer. We design a test page to directly capture the profile of each isolated dot. The idea is similar to [10, 20]. Whereas the main concern of [10, 20] is the dot displacement, our focus is the dot profile. Fig. 1 (a) shows a digital test patch. It contains a binary bitmap where only every 7-th column and 7-th row contains 1's. There are 15 such patches on the test page.

The test page is first printed at 1200 dpi by a prototype pagewide printhead manufactured by HP Inc.. So in the remainder of this paper, $1/X = 1200$ dpi. Then, the printout is captured with a QEA PIAS-II camera at 7663.4 dpi. Each test patch fits entirely in the field of view of the camera, so 15 captures are needed for a printed page. Each printer pixel corresponds to $\frac{7663.4}{1200} \times \frac{7663.4}{1200} \approx 6.39 \times 6.39$ camera pixels. To facilitate the subsequent analysis, we convert this ratio to an integer, i.e. 6×6. We exploit the approach presented in [19] to transform the camera pixels into ultra high definition (UHD) pixels of size $\frac{1}{7200} \times \frac{1}{7200}$ in^2 via

$$c'[i',j'] = \sum_{[i,j] \in \Omega_{i',j'}} \alpha_{i',j'}[i,j]c[i,j], \tag{1}$$

where $c'[i',j']$ is the absorptance of the estimated UHD pixel, $\Omega_{i',j'}$ denotes a set of camera pixels $c[i,j]$ intersecting with the UHD pixel $c'[i',j']$, and $\alpha_{i',j'}[i,j]$ is the intersection ratio. The validity of this transformation lies with the assumption that by definition, the UHD lattice is aligned with the printer lattice, and the camera lattice is not rotated or skewed with respect to the printer lattice. Horizontal or vertical displacement of the camera lattice with respect to the printer lattice can be estimated from the L-shaped patterns located on both sides of the bottom of the test patch shown in Fig. 1. Next, the segmentation mask is computed according to Otsu's method [21]. Shown in Figs. 1 (b) and (c) are the transformed image of the test patch and its corresponding segmentation mask. Finally, the sample mean and standard deviation profiles of all the 3300 dots on the printed test page are computed. The contour plots are presented in Fig. 2.

As can be seen from Fig. 2 (a), the mean dot is limited to a 5×3 printer-pixel region, being slightly elongated in the vertical direction. Besides, the shade is relatively dark in the center and becomes lighter towards the edge. Looking at Fig. 2 (b), we note that the standard deviation is the greatest around the shoulder of the dot, i.e. where the absorptance is changing most rapidly from 0.7 to 0.1 as we go from the center of the dot to the periphery. Nevertheless, the maximum standard deviation is just 0.009. Therefore, it is reasonable to assume that the dots produced by the print bar are constant in shape, and equal to the mean profile.

Overview of DBS

DBS is a search-based algorithm that uses a human visual system (HVS) model [22] $h(x,y)$ to find a halftone image $g(x,y)$ that minimizes the visual error between the perceived halftone image $\tilde{g}(x,y)$ and the perceived continuous-tone image $\tilde{f}(x,y)$. The error metric is

$$E = \int_{x,y} \left|\tilde{g}(x,y) - \tilde{f}(x,y)\right|^2 \mathrm{d}x\,\mathrm{d}y. \tag{2}$$

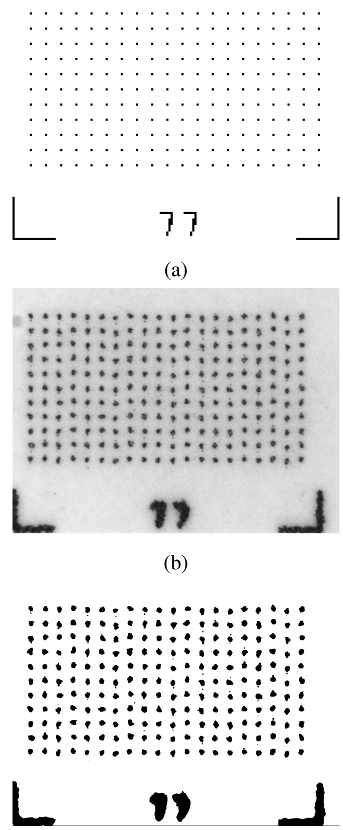

(a) (b) (c)

Figure 1: (a) A digital test patch. (b) The printed test patch captured at 7336.4 dpi and converted to 7200 dpi. (c) The binary segmentation mask of the test patch.

To achieve the local minimum, DBS iteratively toggles a pixel or swaps it with a neighboring pixel that has a different value.

Suppose there exists an ideal printer whose dot profile $p(x,y) = \mathrm{rect}(\frac{x}{X}, \frac{y}{X})$. Let $g[m,n]$ denote the digital halftone image. Then, the perceived halftone rendered by the printer is

$$\tilde{g}(x,y) = \sum_{m,n} g[m,n] \cdot \tilde{p}(x - mX, y - nX), \tag{3}$$

where $\tilde{p}(x,y) = h(x,y) * p(x,y) \approx h(x,y)$ [8] denotes the cascade of the dot profile with the HVS. The closed-form expression of $h(x,y)$ can be found in [23]. Similarly, $\tilde{f}(x,y)$ can be represented in terms of $f[m,n]$. Define $e[m,n] = g[m,n] - f[m,n]$. Then, (2) can be written as

$$E = \sum_{m,n} \sum_{k,l} e[m,n]e[k,l]c_{\tilde{p}\tilde{p}}[m-k, n-l], \tag{4}$$

where $c_{\tilde{p}\tilde{p}}(x,y) = \int_{\xi,\eta} \tilde{p}(\xi,\eta) \cdot \tilde{p}(\xi + x, \eta + y)\,\mathrm{d}\xi\,\mathrm{d}\eta$ is the autocorrelation function of $\tilde{p}(x,y)$, and $c_{\tilde{p}\tilde{p}}[m,n] = c_{\tilde{p}\tilde{p}}(mX, nX)$ is the sampled version of it.

Dot Profile Model

Based on the dot statistics in Sec. Printer Characterization, a dot profile model is developed to summarize the characteristics of the target printer. It is assumed that the printer is capable of

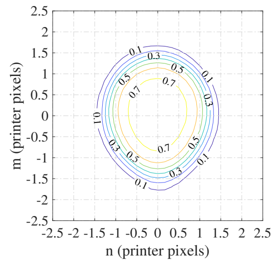

(a)

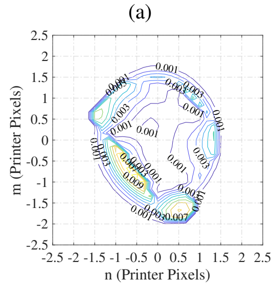

(b)

Figure 2: (a) The mean dot profile and (b) standard deviation profile in the units of absorptance.

ejecting consistent ink drops at designated locations. The size, shape, and the absorption uniformity of the drops are the same as those of the mean dot. The effect of dot overlap is modeled as addition with saturation to 1 (full black). Under this model, the rendered halftone image produced by the target printer can be simulated as a function of the mean dot profile and the digital halftone. We build a 7200 dpi simulated printer based upon this model with the UHD mean dot profile.

To embed the printer model in DBS, [8] and [10] create an equivalent gray-scale (EQGS) image. It is computed as

$$\bar{g}_{\mathrm{SD}}[m,n] = \frac{1}{X^2}\int_{\Omega^{\mathrm{SD}}[m,n]} g(x,y)\,\mathrm{d}x\,\mathrm{d}y, \tag{5}$$

where $\Omega^{\mathrm{SD}}[m,n]$ is a printer cell of size $\frac{1}{1200}\times\frac{1}{1200}$ in^2 centered at $(mX+\frac{X}{2}, nX+\frac{X}{2})$, where as stated before $1/X = 1200$ dpi. We refer to $\bar{g}_{\mathrm{SD}}[m,n]$ as the SD EQGS image. Following the lead of these earlier works, we too use the EQGS image to measure the visual fidelity of the printed halftone to the original image.

Before incorporating the SD EQGS image in DBS, we use the simulated printer to examine its validity. Shown in Fig. 3 (a)-(c) are a bitmap, its simulated print, and the SD EQGS image. It can be observed that the SD EQGS image provides a reasonable approximation to dot overlap; but it is not good at depicting the edges and details. Therefore, it is necessary to refine the estimation. We develop an HD EQGS image by partitioning each printer pixel into 3×3 sub-pixels. The HD EQGS value is then computed within each $\frac{X}{3}\times\frac{X}{3}$ cell. This process raises the resolution of the EQGS image to 3600 dpi. The resulting HD EQGS image is shown in Fig. 3 (d).

Along the lines of the tabular approaches [8–10], an EQGS LUT will be precomputed. With our target printer, the EQGS value of a pixel can be determined in a 5×3 region, so there will be 2^{15} possible binary patterns. In this case, the approach in [8] is intractable, because one would need to manually capture lots of patterns. This necessitates the use of an analytical printer model. To minimize the measurements, we simulate the printed image of all these patterns using the simulated printer, and then compute the EQGS values digitally. In so doing, the LUT can easily be obtained. The algorithm for generating the LUT is summarized below. It is worth mentioning that each entry of the SD LUT is a single value, whereas that of the HD LUT is a 9-element array.

Algorithm 1: Computation of the LUT

```
Initialize the UHD image ḡ_UHD ← 0;
Initialize the table LUT ← 0;
for i ← 0 to 2^15 − 1 do
    Convert i to a 5 × 3 binary bitmap B;
    for b ∈ B do
        if b == 1 then
            Add the UHD dot profile to ḡ_UHD on the
              corresponding location;
    if ḡ_UHD[:,:] > 1 then
        ḡ_UHD[:,:] ← 1;
    LUT[i,:] ←average value of the UHD pixels within
      the center pixel on the SD or HD lattice;
return LUT;
```

Dot Profile Model-based DBS

In this section, we show a detailed formulation of DBS with the HD dot profile model. The SD case can be easily derived from the HD case; so it is omitted here. Let S denote the upsampling factor. i.e. $S=1$ for SD and $S=3$ for HD. The perceived HD EQGS image is given by

$$\bar{g}_{\mathrm{HD}}(x,y) = \sum_{u,v}\bar{g}_{\mathrm{HD}}[u,v]\cdot\tilde{p}_{\mathrm{HD}}\left(x-u\frac{X}{S}, y-v\frac{X}{S}\right). \tag{6}$$

Here the HD EQGS image $\bar{g}_{\mathrm{HD}}[u,v] = \frac{1}{7200^2}\int_{\Omega^{\mathrm{HD}}[u,v]} g(x,y)\,\mathrm{d}x\,\mathrm{d}y$, where $\Omega^{\mathrm{HD}}[u,v]$ is an HD cell of size $\frac{1}{7200}\times\frac{1}{7200}$ in^2. Define the discretized and truncated version of the perceived dot profile $\tilde{p}_{\mathrm{HD}}[u,v] = \tilde{p}_{\mathrm{HD}}\left(x-u\frac{X}{S}, y-v\frac{X}{S}\right)$. Then,

$$E = \sum_{u,v}\sum_{s,t}\bar{e}_{\mathrm{HD}}[u,v]\bar{e}_{\mathrm{HD}}[s,t]c_{\tilde{p}_{\mathrm{HD}}\tilde{p}_{\mathrm{HD}}}[u-s,v-t], \tag{7}$$

where $\bar{e}_{\mathrm{HD}}[u,v] = \bar{g}_{\mathrm{HD}}[u,v] - f_{\mathrm{HD}}[u,v]$.

Let us consider the effect of changing the state of halftone pixels on the cost value. Let $\mathcal{N}^{\mathrm{HD}}[u,v]$ denote the pixels in the 5×3 neighborhood of $[u,v]$. Toggling $[m_0,n_0]$ or swapping $[m_0,n_0]$ and $[m_1,n_1]$ in the halftone will affect the EQGS values of pixels in $\mathcal{N}^{\mathrm{HD}}_{\mathrm{accepted}} \triangleq \mathcal{N}^{\mathrm{HD}}[u_0,v_0]\cup\mathcal{N}^{\mathrm{HD}}[u_1,v_1]$. Given the fact that the input image $f_{\mathrm{HD}}[u,v]$ does not change, the new error image will be

$$\bar{e}'_{\mathrm{HD}}[u,v] = \begin{cases}\bar{e}_{\mathrm{HD}}[u,v]+\Delta\bar{g}_{\mathrm{HD}}[u,v], & \text{for } [u,v]\in\mathcal{N}^{\mathrm{HD}}_{\mathrm{accepted}},\\ \bar{e}_{\mathrm{HD}}[u,v], & \text{otherwise.}\end{cases} \tag{8}$$

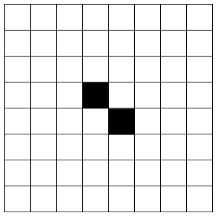

(a)

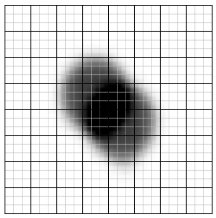

(b)

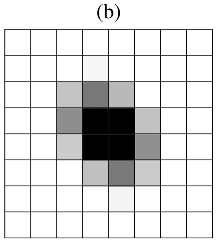

(c)

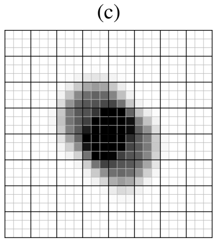

(d)

Figure 3: Development of the SD and HD EQGS images. The black lines denote the printer lattice, and the gray lines denote the HD lattice. (a) Original digital halftone image sent to the simulated printer. (b) Rendered image at 7200 dpi. (c) SD EQGS image at 1200 dpi. (d) HD EQGS image at 3600 dpi.

Thus, the new cost is

$$\begin{aligned}E' &= \sum_{u,v}\sum_{s,t}\tilde{e}'_{\mathrm{HD}}[u,v]\tilde{e}'_{\mathrm{HD}}[s,t]c_{\tilde{p}_{\mathrm{HD}}\tilde{p}_{\mathrm{HD}}}[u-s,v-t] \\ &= E + \sum_{[u,v]\in\mathcal{N}^{\mathrm{HD}}_{\mathrm{accepted}}}\ \sum_{[s,t]\in\mathcal{N}^{\mathrm{HD}}_{\mathrm{accepted}}} \Delta\tilde{g}_{\mathrm{HD}}[u,v]\Delta\tilde{g}_{\mathrm{HD}}[s,t] \\ &\qquad \times c_{\tilde{p}_{\mathrm{HD}}\tilde{p}_{\mathrm{HD}}}[u-s,v-t] \\ &\quad + 2\sum_{[u,v]\in\mathcal{N}^{\mathrm{HD}}_{\mathrm{accepted}}}\ \sum_{s,t}\Delta\tilde{g}_{\mathrm{HD}}[u,v]\tilde{e}_{\mathrm{HD}}[s,t] \\ &\qquad \times c_{\tilde{p}_{\mathrm{HD}}\tilde{p}_{\mathrm{HD}}}[u-s,v-t].\end{aligned} \tag{9}$$

We further define $c_{\tilde{p}_{\mathrm{HD}}\tilde{e}_{\mathrm{HD}}}[u,v] = \sum_{s,t}\tilde{e}_{\mathrm{HD}}[u,v]c_{\tilde{p}_{\mathrm{HD}}\tilde{p}_{\mathrm{HD}}}[u-s,v-t]$. Therefore, the change in the cost due to a trial toggle/swap can be written as

$$\begin{aligned}\Delta E = &\sum_{[u,v]\in\mathcal{N}^{\mathrm{HD}}_{\mathrm{accepted}}}\ \sum_{[s,t]\in\mathcal{N}^{\mathrm{HD}}_{\mathrm{accepted}}} (\Delta\tilde{g}_{\mathrm{HD}}[u,v]\Delta\tilde{g}_{\mathrm{HD}}[s,t]) \\ &\qquad \times c_{\tilde{p}_{\mathrm{HD}}\tilde{p}_{\mathrm{HD}}}[u-s,v-t] \\ &+ 2\sum_{[u,v]\in\mathcal{N}^{\mathrm{HD}}_{\mathrm{accepted}}} \Delta\tilde{g}_{\mathrm{HD}}[u,v]c_{\tilde{p}_{\mathrm{HD}}\tilde{e}_{\mathrm{HD}}}[u,v].\end{aligned} \tag{10}$$

This error metric will guide the search of DBS. Note that $c_{\tilde{p}_{\mathrm{HD}}\tilde{p}_{\mathrm{HD}}}[u,v]$ is independent of the change, but if a change is accepted, $c_{\tilde{p}_{\mathrm{HD}}\tilde{e}_{\mathrm{HD}}}[u,v]$ needs to be updated by

$$\begin{aligned}&c'_{\tilde{p}_{\mathrm{HD}}\tilde{e}_{\mathrm{HD}}}[u,v] \\ =&c_{\tilde{p}_{\mathrm{HD}}\tilde{e}_{\mathrm{HD}}}[u,v] + \sum_{[s,t]\in\mathcal{N}^{\mathrm{HD}}_{\mathrm{accepted}}} \Delta\tilde{g}_{\mathrm{HD}}[s,t]c_{\tilde{p}_{\mathrm{HD}}\tilde{p}_{\mathrm{HD}}}[u-s,v-t].\end{aligned} \tag{11}$$

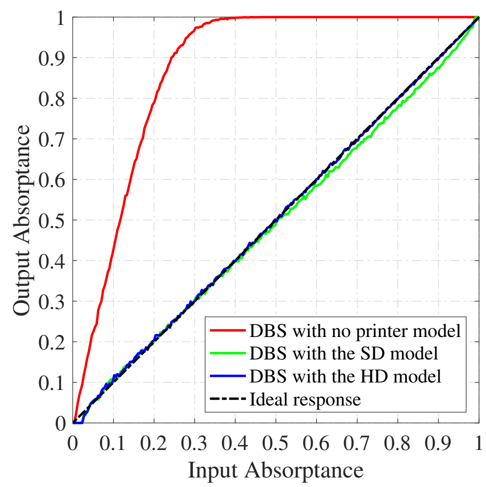

(a)

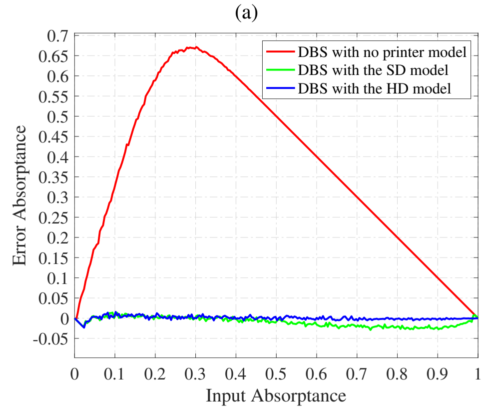

(b)

Figure 4: (a) Tone reproduction curves and (b) tone error curves of DBS with no printer model, DBS with the SD model, and DBS with the HD model. Note that the output absorptance is calculated based on the simulated output of the halftones of constant-tone patches, and the tonal error is obtained by subtracting the input absorptance from the output absorptance.

Experimental Results

In this section, the effect of incorporating the printer models in DBS is evaluated. Tone curves calculated according to [24] are shown in Fig. 4. As can be seen, the reproduction curve of DBS with no model, indicated by a red line, is severely distorted. It can be also seen that after embedding the printer models, the bias becomes negligibly small. This suggests that both models can produce a correct average tone at most levels. It is noteworthy that the tone reproduction curves for both models contain a small flat region in the very highlights. This will result in a decrease in absorptance that can merely be rectified by applying the inverse mapping of the tone reproduction curve, namely tone correction.

Fig. 5 shows the comparison of the simulated prints of a halftone generated by DBS with no model, with the SD model, and with the HD model. To present a fair comparison, tone correction was applied in all three cases before halftoning. These images were all printed at 7200 dpi using the simulated dot profile printer. It can be observed that the graininess in the mid-tone and shadow regions in (a) becomes less noticeable in both (b) and (c). This implies that the irregularly shaped dots were properly controlled by the models. Looking at the highlights, i.e. the sky area, we note that the improvement is less significant. We believe the reason is that there are fewer overlapping dots, and thus tone compensation should suffice to reduce the bias. Comparing (b) and (c), we note that the HD model performs better than the SD model in the midtones and in the shadow regions, i.e. the side of the aircraft and the lawn. The halftone structures are less visible and more homogenous, making the overall appearance more visually pleasing. There is also more detail in the landing gear with the HD model.

Conclusion

We characterized a printer by measuring and analyzing the dot profiles. Based on the dot statistics, we built a simulated printer to simulate the appearance of the rendered images produced by this printer. The model parameters were computed analytically, so the number of measurements was greatly reduced. We incorporated both the SD and HD printer models in DBS. With the two models, DBS effectively ameliorates the noisiness, and yields nearly linear tone reproduction without tone correction. The HD model outperformed the SD model in the midtones and in the shadows.

References

[1] J. P. Allebach, "DBS: retrospective and future directions," in *Proc. SPIE Color Imaging: Device-Independent Color, Color Hardcopy, Graphic Arts VI*, vol. 4300, Jan. 2001, pp. 358–376.

[2] T. N. Pappas and D. L. Neuhoff, "Model-based halftoning," in *Proc. SPIE Human Vis., Visual Process., Digit. Display II*, vol. 1453, Feb. 1991, pp. 244–255.

[3] J. P. Allebach, "Binary display of images when spot size exceeds step size," *Appl. Opt.*, vol. 19, no. 15, pp. 2513–2519, Aug. 1980.

[4] P. Stucki, "MECCA–A multiple-error correcting computation algorithm for bilevel image hardcopy reproduction," IBM Research Laboratory, Zurich, Switzerland, Res. Rep. RZ1060, 1981.

[5] R. L. Stevenson and G. R. Arce, "Binary display of hexagonally sampled continuous-tone images," *J. Opt. Soc. Amer. A, Opt. Image Sci.*, vol. 2, no. 7, pp. 1009–1013, July 1985.

[6] T. N. Pappas and D. L. Neuhoff, "Least-squares model-based halftoning," *IEEE Trans. Image Process.*, vol. 8, no. 8, pp. 1102–1116, Aug. 1999.

[7] M. Analoui and J. P. Allebach, "Model-based halftoning using direct binary search," in *Proc. SPIE, Human Vis., Visual Process., Digit. Display III*, vol. 1666, Feb. 1992, pp. 96–108.

[8] F. A. Baqai and J. P. Allebach, "Halftoning via direct binary search using analytical and stochastic printer models," *IEEE Trans. Image Process.*, vol. 12, no. 1, pp. 1–15, Jan. 2003.

[9] T. N. Pappas, C. Dong, and D. L. Neuhoff, "Measurement of printer parameters for model-based halftoning," *J. Electron. Imaging*, vol. 2, no. 3, pp. 193–204, July 1993.

[10] J.-H. Lee and J. P. Allebach, "Inkjet printer model-based halftoning," *IEEE Trans. Image Process.*, vol. 14, no. 5, pp. 674–689, May 2005.

[11] L. Zhang, A. Veis, R. Ulichney, and J. Allebach, "Binary text image file preprocessing to account for printer dot gain," in *IEEE Int. Conf. Image Process.*, 2014, pp. 2639–2643.

[12] J. Liu, H. Su, W. Hu, L. Zhang, and D. Tao, "A minimal munsell value error based laser printer model," *Elsevier Neurocomputing*, vol. 204, pp. 231–239, 2016.

[13] L. G. Coppel, R. Slavuj, and J. Y. Hardeberg, "Modeling coverage-dependent ink thickness in ink-jet printing," *Appl. Opt.*, vol. 55, no. 5, pp. 1138–1144, 2016.

[14] T. N. Pappas and D. L. Neuhoff, "Printer models and error diffusion," *IEEE Trans. Image Process.*, vol. 4, no. 1, pp. 66–80, Jan. 1995.

[15] S. J. Park, M. Q. Shaw, G. Kerby, T. Nelson, D.-Y. Tzeng, K. R. Bengtson, and J. P. Allebach, "Halftone blending between smooth and detail screens to improve print quality with electrophotographic printers," *IEEE Trans. Image Process.*, vol. 25, no. 2, pp. 601–614, 2015.

[16] S. Wang, "Aerodynamic effect on inkjet main drop and satellite dot placement," in *Proc. IS&T NIP & Digit. Fabrication Conf.*, 1998, pp. 5–8.

[17] Z. Wang and E. A. Elsayed, "Degradation modeling and prediction of ink fading and diffusion of printed images," *IEEE Trans. Rel.*, vol. 67, no. 1, pp. 184–195, 2018.

[18] P. D. Fleming, J. E. Cawthorne, F. Mehta, S. Halwawala, and M. K. Joyce, "Interpretation of dot fidelity of ink jet dots based on image analysis," *J. Imaging Sci. Technol.*, vol. 47, no. 5, pp. 394–399, Sep. 2003.

[19] Y. Ju, T. Kashti, T. Frank, D. Kella, D. Shaked, M. Fischer, R. Ulichney, and J. P. Allebach, "Black-box models for laser electrophotographic printers– Recent progress," in *Proc. IS&T 29th Int. Conf. Digit. Printing Technol.*, Sep. 2013, pp. 66–71.

[20] Y. Mao, "Digital imaging and halftoning algorithms design: Parallel processing, printed image artifacts modeling, and learning-based image analysis," Ph.D. dissertation, Dept. Elect. Comput. Eng., Purdue Univ., West Lafayette, IN, USA, Dec. 2021.

[21] N. Otsu, "A threshold selection method from gray-level histograms," *IEEE Trans. Syst. Man Cybern. Syst.*, vol. 9, no. 1, pp. 62–66, Jan. 1979.

[22] R. Näsänen, "Visibility of halftone dot textures," *IEEE Trans. Syst. Man Cybern. Syst.*, vol. 14, no. 6, pp. 920–924, 1984.

[23] C. Lee, "Hybrid screen design and automatic portrait im-

age enhancement," Ph.D. dissertation, Dept. Elect. Comput. Eng., Purdue Univ., West Lafayette, IN, USA, Dec. 2008.
[24] D. J. Lieberman and J. P. Allebach, "A dual interpretation for direct binary search and its implications for tone reproduction and texture quality," *IEEE Trans. Image Process.*, vol. 9, no. 11, pp. 1950–1963, Nov. 2000.

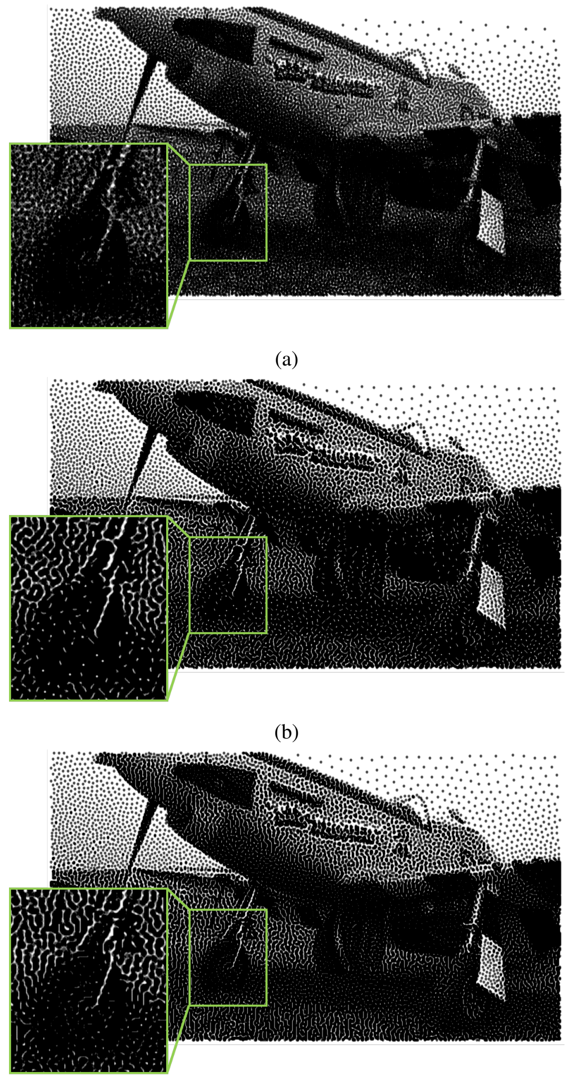

(a)

(b)

(c)

Figure 5: Simulated results printed at 7200 dpi. The halftone images are generated by DBS with (a) no printer model, (b) the SD model, and (c) the HD model. It is recommended to set the zoom level to 150% and to view these images at about 12 inches. Note from the call-outs that the HD model shows the most detail in the landing gear.